

# Robust Protein Electrical Junctions with Permanent Contacts show Activation-less Charge Transport down to 10 K

Shailendra K. Saxena<sup>1,2</sup>, Sudipta Bera<sup>1</sup>, Tatyana Bendikov<sup>3</sup>, Israel Pecht<sup>4</sup> Mordechai Sheves<sup>1\*</sup>,  
David Cahen<sup>1\*</sup>

## Affiliations:

<sup>1</sup> Department of Molecular Chemistry & Materials Science, Weizmann Institute of Science, Rehovot, Israel.

<sup>2</sup> Department of Physics and Nanotechnology, College of Engineering and Technology, SRM Institute of Science and Technology, Kattankulathur, Chennai Tamil Nadu, India.

<sup>3</sup> Department of Chemical Research Support, Weizmann Institute of Science, Rehovot Israel

<sup>4</sup> Department of Immunology & Regenerative Biology, Weizmann Institute of Science, Rehovot, Israel.

\*corresponding authors, [david.cahen@weizmann.ac.il](mailto:david.cahen@weizmann.ac.il), [mudi.sheves@weizmann.ac.il](mailto:mudi.sheves@weizmann.ac.il)

## ORCID:

Shailendra K. Saxena: 0000-0001-7156-3407

Sudipta Bera: 0000-0001-7894-9249

Tatyana Bendikov: 0000-0002-1637-6366

David Cahen: 0000-0001-8118-5446

Mordechai Sheves: 0000-0002-5048-8169

Israel Pecht: 0000-0002-1883-9547

## **Abstract**

Robust solid-state protein junctions (RPJs) with permanent contacts are essential for a wide range of studies aimed at elucidating the mechanisms for electron transport across such junctions and their possible applications. Here we report on first time, RPJs formed with vacuum-evaporated carbon (eC) followed by Au as top electrode set on a single bilayer of bacteriorhodopsin (bR), self-assembled from solution on an Au substrate. The light-induced photocycle of bR, as well as the amide I & II vibrational frequencies of bR, were unchanged upon eC deposition; the yield of the resulting junctions was reproducible ~ 90 % (non-shortcd), and they were stable between ~ 10 and 300K. The current-voltage characteristics of these junctions were temperature-independent and the junctions were stable for several months. Hence, such robust all-solid-state protein junctions provide valuable tools for investigating the potential use of proteins in future bio-molecular electronic devices.

**Keywords:** Bioelectronic, Molecular Electronic, Solid State, Bacteriorhodopsin, Carbon

Proteins, with their diverse structures and functions, offer a promising avenue for creating bio-compatible electronic devices. In bio-electronics, molecules, particularly proteins, are integrated into electronic devices for various applications as active, electronically conducting components, such as sensors, transistors, and even entire circuits<sup>1</sup>. The finding that ultra-thin protein films can conduct electrons opens the exceptional potential for harnessing the diverse properties of proteins, such as chemical specificity and self-assembly, to their employment in electronics. Such use will enable the development of sensitive, selective, and adaptable devices that can interface seamlessly with biological systems, paving new ways for innovations in diagnostics, drug delivery, and personalized medicine on a molecular scale.

Charge transport through protein junctions implies the flow of e.g., electrons, where the proteins act as conduits for electronic communication. These junctions can leverage the unique properties inherent in proteins in molecular-scale electronic devices. Electronic charges can flow by hopping<sup>2</sup> between amino acids or amino acids and co-factors or by tunnelling<sup>[3,4]</sup> through the protein matrix, controlled by structural and environmental properties. Resolving the mechanisms controlling charge transport via protein junctions is pivotal for developing efficient bio-electronic devices. Investigating charge transport through such biomolecules in a solid state junction<sup>5-7</sup> may open novel avenues for bioelectronics and nanotechnology. Among the

unanswered questions in understanding protein electronics<sup>8-10</sup>, we note the following ones: (i) What is the charge transport mechanism, taking into account the unusual observation of temperature-independent currents proceeding through > 4-5 nm thick protein junctions? (ii) How can one fabricate robust protein junctions (RPJs) for real-world applications? Specifically, we need junctions that should be sufficiently stable for long-term measurements, e.g., for low-temperature probe stations, in strong magnetic fields, under hydrostatic pressure, or in specialized spectroscopic cells required for investigating the transport.

Top electrodes were shown earlier to be produced successfully by evaporating carbon (eC) followed by gold (Au) fabricating molecular junctions with conjugated organic molecules, which were shown to maintain their molecular properties<sup>11,12</sup>. Here we show progress in sample robustness by contacting proteins, soft, non-rigid macromolecules, with eC. The employed protein is bacteriorhodopsin treated with the detergent octylthioglucoside (OTG)<sup>10,13,14</sup>. The OTG treatment leads to partially native lipid depleted vesicles, that collapse upon deposition onto a substrate, forming well-reproducible, uniform bR bi-layers<sup>10,15</sup>. For simplicity, such bR bilayer will be referred to as a bR single layer, (SL), in the entire manuscript. We chose bR for several reasons: (i) it is a relatively thermally stable; (ii) it has a photochemically-driven optical signature (explained in a later section), which is sensitive to its native

conformation and, therefore, provides information on its conformation in the junction. Four  $\mu\text{m}$  wide Au lines provide the bottom electrodes, on which the bR bilayer forms, likely produced by collapse of the resulting bR vesicles as we have shown earlier<sup>15,16</sup>. Subsequently, the 50  $\mu\text{m}$  wide top electrode of 10 nm eC and 30 nm Au was vacuum deposited on the protein. The resulting  $4 \times 50 \mu\text{m}^2$  (lateral dimensions) protein junctions were used for further study. Details on device fabrication are presented in the supporting information.

A crucial issue for any new process of making electronic contact to proteins is to check whether the fabrication damages the protein. As noted, the as-deposited bR film is a single bR-bR bilayer, an SL, without any OTG, but with some native lipids left<sup>14</sup>. It forms on the surface of the Au bottom matrix, derivatized with a covalently bound via an Au-S bond monolayer of cysteamine. Protein-cysteamine attachment is by electrostatic adsorption upon exposure to the bR solution (see experimental section). Formation of the bR SL was confirmed first by ellipsometry, followed by atomic force microscopy (AFM) scratching<sup>17</sup>, following our earlier described protocol. The SL thickness was found to be 9.2 nm by ellipsometry (on a test sample) and 9.6 nm by AFM, which are in good agreement with previously reported studies<sup>15</sup>.

Figure 1(A) shows the surface topography of the bR SL. The granular features of the protein are visible, spread over the gold surface. To ascertain that the bR remains functional, after binding to the surface, its photocycle was monitored. To perform

this experiment, a bR SL was formed on the optically transparent substrate of indium tin oxide (ITO), also via electrostatic interaction, but with 3-Aminopropyl trimethoxysilane (APTMS) as linker (see experimental section). Following light absorption, bacteriorhodopsin is converted to a series of intermediates with well-defined lifetimes and spectral properties<sup>18</sup>. When exposed to > 500 nm light wavelength, bR converts to an ‘intermediate state’ that absorbs at 412 instead of 568 nm, called M-state (412). From this state, bR returns to its original state (that absorbs at 568 nm) by thermal relaxation or exposure to blue light (i.e., light absorbed by the M-state). Optical absorption measurements were performed on the bR SL on ITO as follows: first a spectrum of the sample was measured in the dark state (“dark1”), followed by absorption measurement under illumination with yellow light (> 500 nm), (“light”). The sample absorption was finally measured after a thermal decay for 2 minutes in the dark (“dark2), which was found to be the same as “dark1”. Difference spectra were obtained by subtracting “dark1” from “light” (blue curve) and “light” from “dark2” (red curve) and are shown in Fig 1 (B). The appearance of a 412 nm peak (with yellow light) and disappearance of the 568 nm peak and the return to its original state illustrate the biological photocycle of bacteriorhodopsin, confirming that the conformation of the bR has not been significantly affected by its deposition as a dry (except for structural water) film.

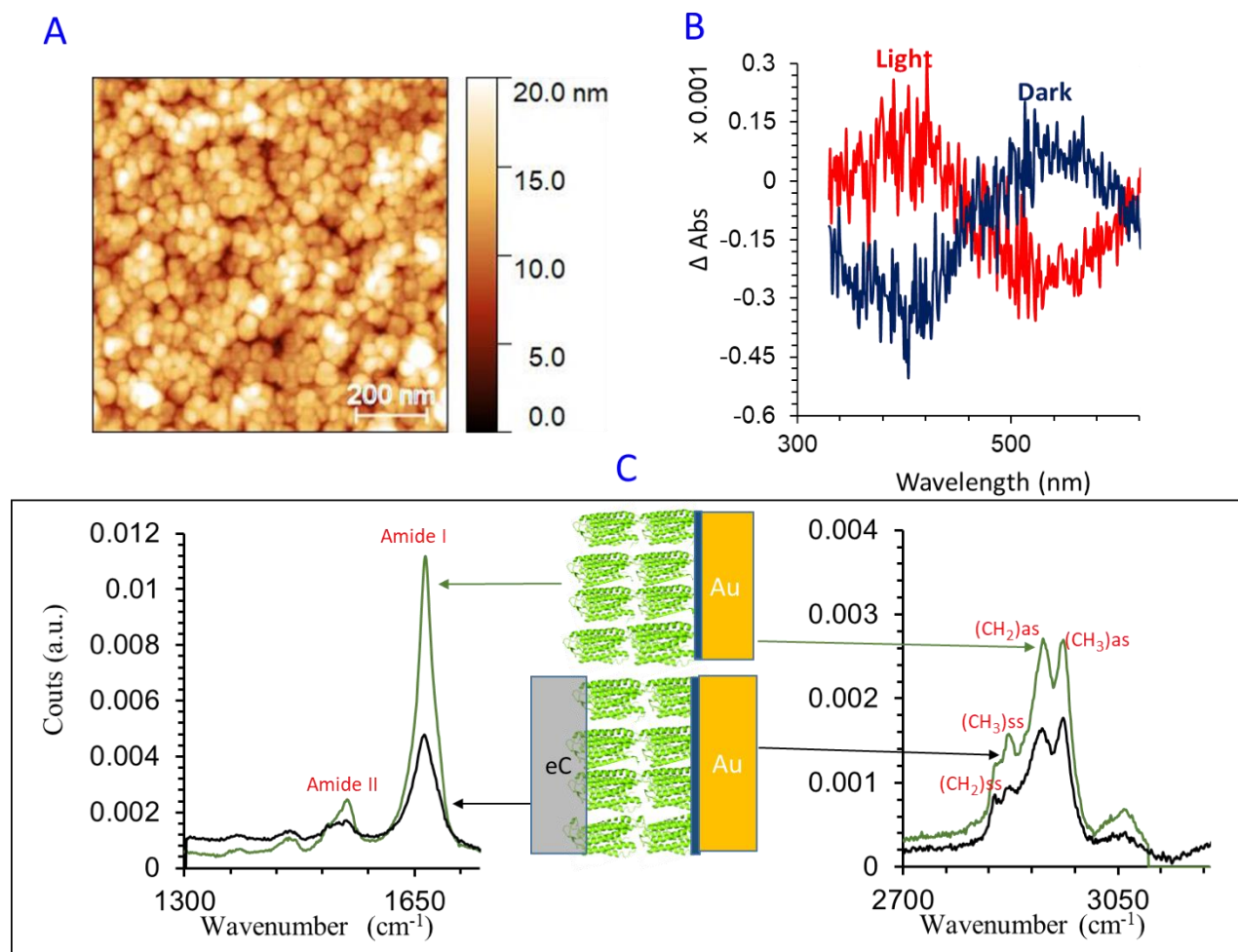


Figure 1. (A) Surface morphology of bR SL (bilayer) showing the protein's granular features, which is ascribed to collapsed vesicles. The rms roughness was  $\sim 2.2$  nm and the coverage was  $> 95\%$ . (B) Optical absorption difference spectra of bR SL on ITO substrate following irradiation with  $> 500$  nm light (red, i.e., light-dark) and 2 minutes in the dark after exposure to light (blue, i.e., dark-light). (C) PM-IRRAS spectra, showing vibrational modes of different groups in bR, including amide I and II peaks (between  $1500$ - $1700$   $\text{cm}^{-1}$ ), before (green) and after C deposition (black).

The state of the protein's structure was further characterized by measuring the IR spectrum of a bR SL on gold, focussing on the amide I and amide II bands, using polarization modulation-infrared reflection-adsorption spectroscopy (PM-IRRAS), as described elsewhere<sup>10</sup>. Figure 1(C) shows the measured spectra, including amide

I and II vibrational peaks at  $1665\text{ cm}^{-1}$  and  $1545\text{ cm}^{-1}$ , respectively (green trace in Fig. 1 (C)). The presence of these peaks supports that the native bR structure is maintained during SL formation on the Au substrate.

After characterization of the protein layer's properties and confirmation of its native conformation, a 10 nm carbon layer was deposited by e-beam evaporation at  $10^{-6}$  mbar. The evaporated carbon (eC) atoms/clusters are very reactive and are expected to react with the outer-most exposed atoms of the protein and remain there, rather than penetrating further into it.<sup>19</sup> Subsequently arriving carbon atoms/clusters will deposit on top of the protein layer, with which they likely have reacted. If this reaction is limited to, say, the first few tenths of nm of the  $>9$  nm film, the eC contacting layer on the protein may well leave the conformation of most of the proteins unchanged.

Non-destructive eC deposition has been reported on very thin ( $< 5$  nm) layers of conjugated, rigid organic molecules.<sup>12,20</sup> Based on optical spectroscopy measurements, it was concluded that the eC deposition does not destroy the molecular structure of those  $< 5$  nm thick monolayers.<sup>11,21</sup> Naturally, a protein layer is quite different from “stick”-like organics and is expected to be more sensitive, especially in terms of its conformation, to the deposition of reactive atoms and clusters than rigid conjugated organic molecules. To investigate the effect of the evaporated carbon (eC) on the protein, PM-IRRAS was also performed on a bR layer after eC layer



deposition. The black line in Fig 1(C) shows the protein characteristics following eC deposition; the amide I & amide II peak positions are unchanged from those measured prior to eC deposition, but as expected, their intensity is reduced, because of scattering by the eC. As shown below, the bR photocycle was also shown to be unaffected by the eC deposition.

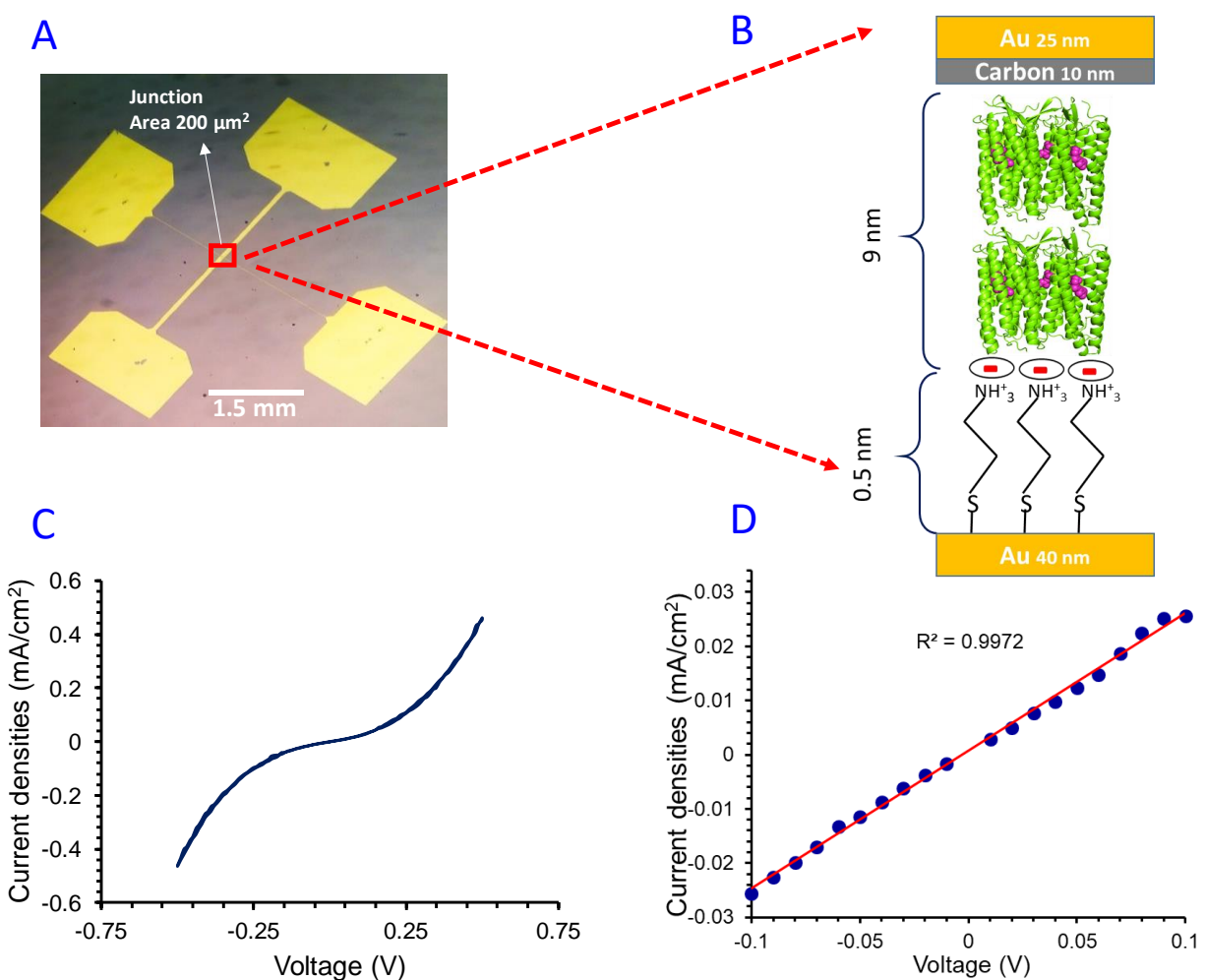


Figure 2. (A) Optical microscopy image of a protein junction; (B) Schematic of bR (PDB 1FBB) junction (not to scale); (C) Room temperature current densities as function of applied bias voltage, J-V, curves; (D) zoom-in on low bias region of plot in panel (C), showing J-V linearity.

To investigate the charge transport via the protein, complete junctions were fabricated. The crosswire geometry that was used to form the junctions is shown in Fig 2 (A). The bottom gold lines (4  $\mu\text{m}$  wide) were modified by binding cysteamine linker molecules followed by bR SL binding to the linker. To complete the crosswire geometry, 50  $\mu\text{m}$  wide top electrodes (of 10 nm eC, followed by 25 nm Au) were deposited perpendicular to the bottom lines, as shown in Fig 2(A). Details of the fabrication method are given in the Supplementary Information. It is worth mentioning that eC contains both  $\text{SP}^2$  and  $\text{SP}^3$  carbons and the ratio of  $\text{SP}^2/\text{SP}^3$  is found to be 3. The supporting X ray photoelectron spectroscopy data (XPS) of eC on Au is given in the supporting information.

The current density-voltage ( $J$ - $V$ ) characteristics of the junctions were studied over the  $\pm 0.5$  V range in medium vacuum ( $<10^{-5}$  mbar). Current densities are calculated using the geometric area ( $\sim 200 \mu\text{m}^2$ ) of the junction. Figure 2(C) presents the current densities of a device measured at room temperature using a two-probe configurations. The differences in characteristics of junctions with and without protein, and with linker monolayer and without it (short circuit) are presented in the Supplementary Information.

The room temperature  $J$ - $V$  curves are non-linear, but nearly symmetric with respect to bias polarity. Current densities are comparable to those reported for bR SL in various other junction configurations<sup>22</sup>. A list, comparing current densities in different configurations, is given in the Supplementary Information. The present Au/protein/eC/Au junctions were found to be very stable within the temperature range 10K-300K, and for the timescale over 3 months. This is illustrated by the  $J$ - $V$  characteristics observed for a freshly prepared junction and those measured after three months (see Supplementary Information).

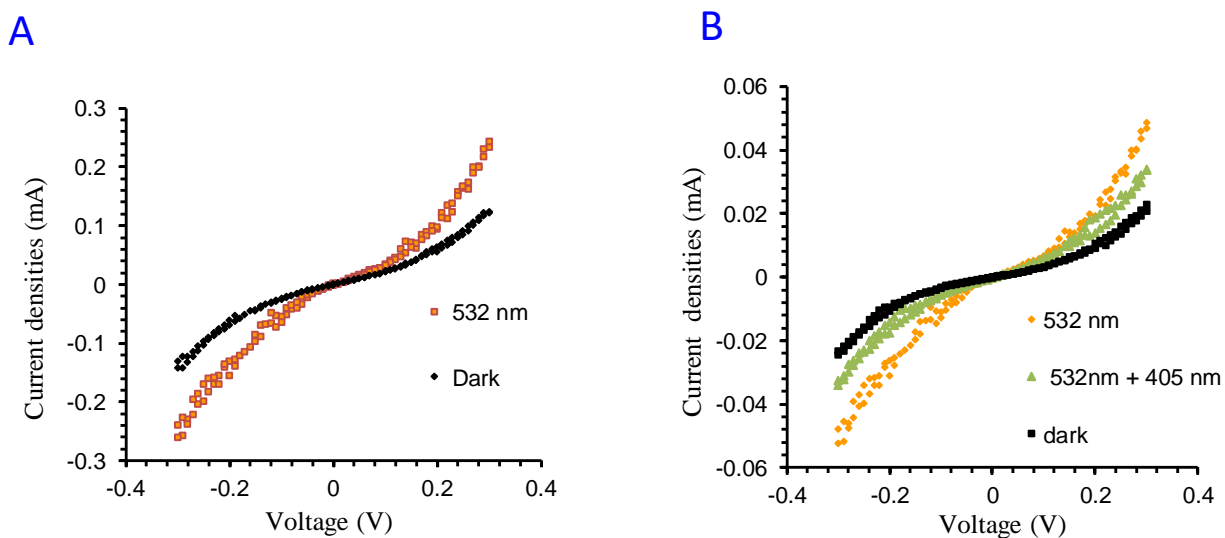


Figure 3 (A):  $I$ - $V$  curves under 532 nm (green) and in the dark (black) (B) same, under 532nm and simultaneous 532 nm and 405 nm illumination (blue), and in dark condition (black).

A key issue regarding the use of solid-state junctions made of protein molecules is whether the protein conformation is significantly affected by the junction fabrication. This question can be effectively answered in the case of bR, as its functionality can be monitored via its photo response, as explained above; the light-induced photocycle of bR is essential for its biological function, pumping protons through its native “purple” membrane. This photo-induced process is known to be affected by significant change in conformation or structure<sup>13,23,24</sup>. Thus, bR optical properties can reflect change in the functionality of the protein caused by eC deposition. In lieu of optical absorption through the top or bottom contacts, which is a challenge for thick enough, to be reasonably conducting, electrodes, we took advantage of bR’s known photoconductivity<sup>25–27</sup>, which follows its light absorption.

Figure 3 shows the *I-V* characteristics measured under different illumination conditions. Such effects on *I-V* characteristics were reported earlier<sup>25,27</sup> for bR junctions with temporary, probe contacts. Enhancement of current was observed with 532 nm light illumination due to accumulation of the photochemically induced intermediate M(412), and the current reverted to its initial dark values upon dark adaptation. The current was partially reverted once a blue light was added to the 532 nm illumination. Fig. 3 shows a similar effect observed here in our protein junction. The junction was illuminated by green light (532 nm), and the current increased from 0.24 nA to 0.52 nA (2.1 times) at 0.3V (Fig. 3A). When the junction was irradiated by a combination

of green and blue light, two effects should proceed simultaneously, namely, transition to the intermediate M(412) state by 532 nm irradiation and partial return to the ground state by blue light. Indeed, we find that only a small enhancement of current (from 0.24 nA to 0.34 nA) i.e., about 1.4 times increase is observed (Fig. 3B), much smaller than that observed upon irradiation by only 532 nm, in agreement with the earlier reports<sup>25,27</sup>. This confirms that protein biological functions are unaffected by the top electrode deposition.

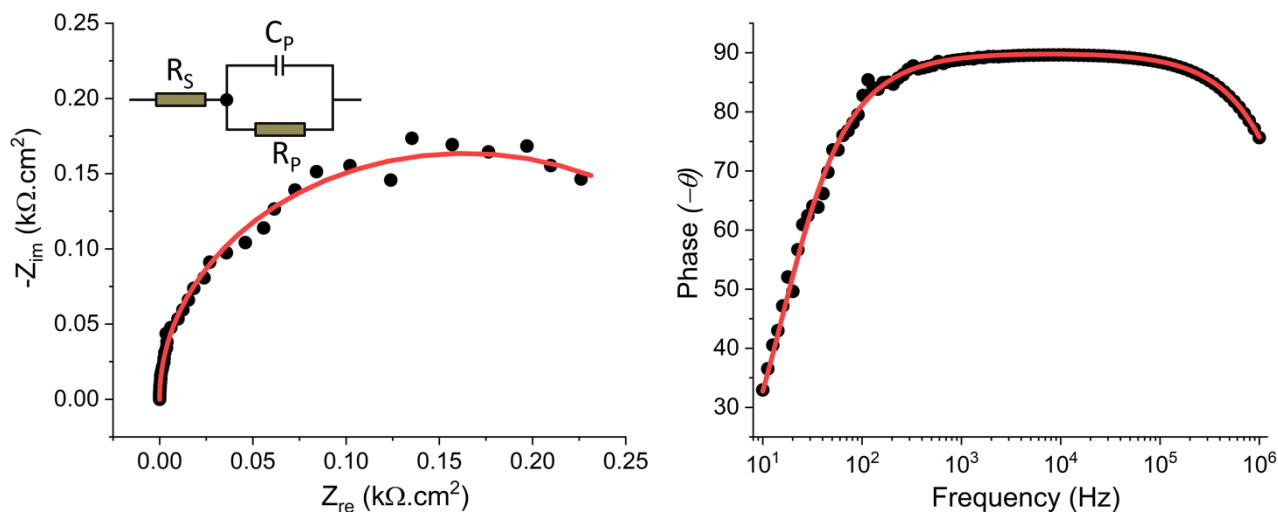


Figure: 4(A) Room temperature ( $293 \pm 2$  K) impedance-based Nyquist plot for a Au/Cys/bR (9 nm)/eC/Au junction over the 10 Hz – 1 MHz frequency range with a 50 mV AC and 0 V DC bias, in low vacuum ( $10^{-3}$  mbar); inset: equivalent circuit used. (B) A part of the Bode plot: impedance phase ( $-\theta$ ) vs.  $\log(\text{frequency})$  for the

Au/Cys/bR (9 nm)/eC/Au junction. Black dots are experimental data, and the red solid lines fit according to the equivalent circuit, shown as inset in (A).

Though the protein layers are densely packed (> 95% coverage), there remains the possibility that evaporation will lead to the growth of carbon filaments through a few nm small voids, which by themselves are unlikely to significantly affect the measurements (discussion in SI of article<sup>28</sup>). Results of the impedance measurements present a non-destructive mode to check for possible conductive filaments present in the protein junction, i.e., in how effective the protein film separates the much higher conductance top and bottom electrodes. Details of the impedance-analyzer-based experimental setup, measurement, and data analysis were presented elsewhere<sup>10</sup>. Here, we can fit the impedance data with a good fitting parameter (chi-square  $\sim 0.005$ ) to a simple equivalent circuit (Inset in Fig. 4A). The Nyquist plot of the bR junctions contains only one nearly perfect part of a semicircle, indicating a single dielectric relaxation process. This Nyquist plot fits well to the same equivalent circuit, which also fits impedance data for the same protein layer between silicon and gold electrodes<sup>10</sup>.

The Bode plot (Fig. 4B) is crucial for our purpose. At a frequency >200 Hz, the phase nearly saturates at a 90° angle, implying fully capacitive behavior of the junctions at high frequencies. It is well known that the parallel R–C circuit typically

behaves as a resistor at low frequencies (ideally  $\theta = 0$ );  $\theta$  should approach  $90^\circ$  at high frequencies when the resultant equivalent circuit is essentially the capacitor<sup>10,29</sup>. Hence, our result shows excellent separation of the junction's top and bottom electrodes by the protein layer, and that any contribution of shorts via pinholes is negligible.

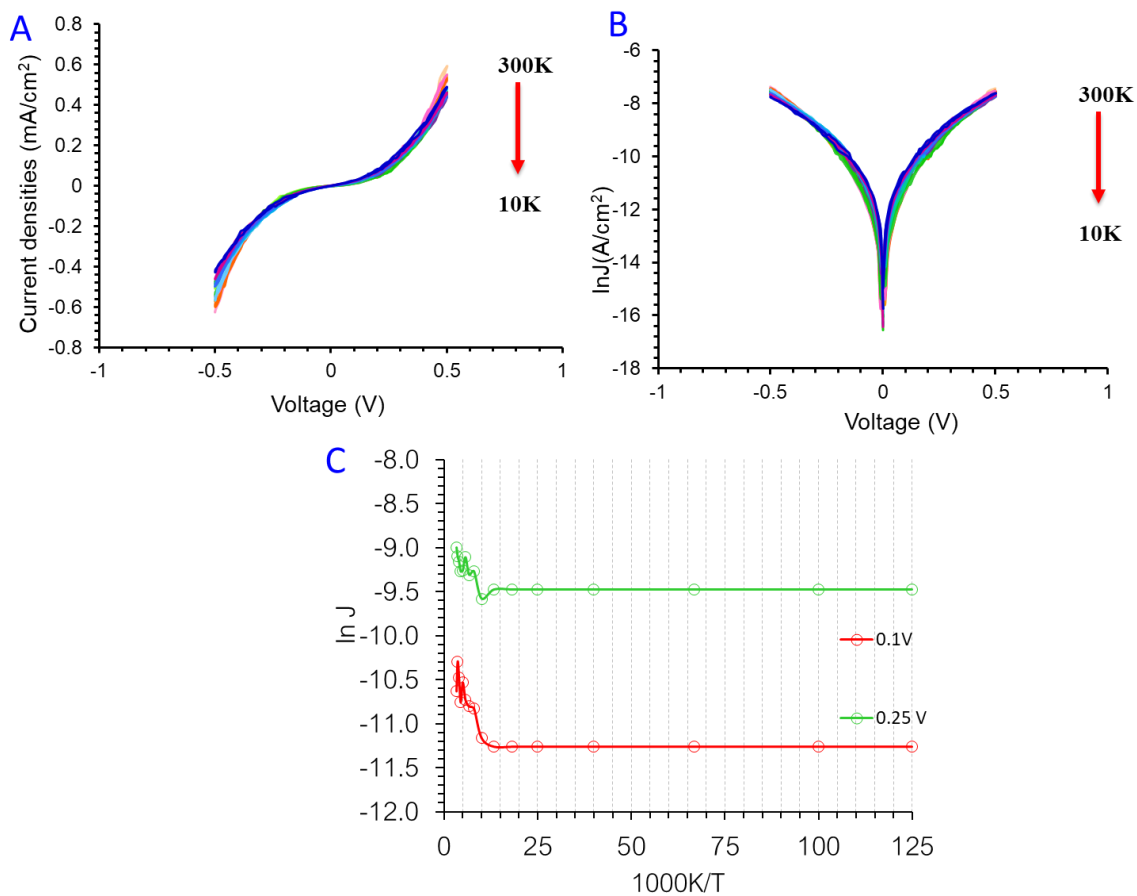


Figure 5. (A) current densities vs bias measured at temperatures from 300K to ~10K; (B) a semi-log plot of the data shown in (A); (C) Arrhenius plot of  $\ln(J)$  vs.  $1000K/T$  for the same data.

Figure 5 (A) shows an overlay of the temperature-dependent current densities ( $J$ - $V$ ) observed via a Au/Cys/bR/C-Au junction. Two distinct regions are seen in these plots, from 300K to 150K and between 100K and 10 K. Between 300K - 200K activation energies of 5.8 and 5.3 meV are found at 0.1 V and 0.25 V, respectively,  $\ll k_B T$  @200K ( $\sim 17$  meV). Any possible thermal activation barrier below  $\sim 100$ K is not measurable. Thus, practically, there is no significant difference in the  $J$ - $V$  characteristics between low and room temperature. Fig. 5(C) shows the data obtained at two different bias voltages as semi-log (Arrhenius) plots. It is worth noting here that junctions were stable at 10K temperature, which shows that they are robust even at lower temperature, i.e., they might be useful also for low temperature bioelectronics. While also the present results, as previous ones<sup>10</sup>, leave the operating charge transport mechanism open, they do show temperature independence of transport across 9-10 nm thick bR layers, is a general result, also if the bottom contact is changed from Si/SiO<sub>x</sub><sup>10</sup> to Au, the linker from APTMS<sup>10</sup> to cysteamine and the top contact from mechanical deposition of a Au pad<sup>10</sup> to evaporated Carbon. The observed distance of the charge transport excludes coherent electron tunnelling. The temperature independence requires temperature-independent nuclear displacement to fit regular hopping and also challenges ideas such as nuclear tunnelling. Notwithstanding this challenge for fundamental understanding, the solid-state robust protein



junction presented here is a most welcome promise for developing future bioelectronics.

Robust, permanently contracted protein junctions have been fabricated. The eC deposition is promising as a top/protecting layer on proteins, enabling stable solid-state junctions/devices. The conformation of the bR proteins inside the junction was not significantly affected following eC deposition. The junction was stable over the 300 K to 10 K temperature range, which gives opportunity to run low temperature experiments. At room temperature in air, the junctions were shown to be stable for several months after fabrication. Temperature-independent currents were found down to 10K.

## **Methods**

bR vesicles were prepared using purple membranes, isolated from *Halobium salinarum* through octylthioglucoside (OTG) treatment, as reported earlier<sup>10</sup>. The bR was preserved in a solution of 10 mM phosphate buffer (PB) containing 0.1 M ammonium sulfate ((NH<sub>4</sub>)<sub>2</sub>SO<sub>4</sub>) at pH 6.4, maintained at room temperature. Subsequently, this solution was diluted with buffer to a concentration of 4 μM for the on-surface immobilization of bR proteins. The resulting solution was used to grow the bR SL on a substrate. There were two parallel experiments

### **1.(a) bR layer formation on gold substrate**

3 nm chromium (Cr) was deposited on clean SiO<sub>x</sub> (300 nm)-on-Si(100) wafer, followed by 50 nm gold. Since there is no exposed thiol residue on bR, a different procedure has been employed for its binding to the flat gold substrate, at a density sufficient for continuous coverage. Thus, cysteamine was employed as a linker to the gold substrates. The substrate was immersed in an 8 mg/mL (approximately 70 mM) aqueous solution of cysteamine hydrochloride (Sigma) for 12 hours to facilitate the binding of Cysteamine via S–Au bonds. Subsequently, the Cysteamine-derivatized Au substrate was washed thoroughly with water, followed by a 1-minute bath sonication with Milli-Q water to eliminate any physisorbed Cysteamine molecules and the surface was then dried with N<sub>2</sub>. The cysteamine-coated gold substrate was immersed in protein solution for 12 hours which resulted in a 9 nm bR layer on the gold substrate. The protein layer was characterized by ellipsometry (J.A. Woollam) to deduce the film thickness, PMIRRAS (single-channel Nicolet 6700 spectrometer with a grazing angle accessory and a liquid nitrogen cooled MCT detector) to measure especially the amide peaks, AFM (using Bruker AFM setup; Nanoscope V Multimode AFM) for surface morphology and thickness, UV-Vis spectroscopy (Agilent photodiode-array spectrophotometer), especially to follow light-induced absorption changes in the protein and a Kratos XPS instrument, especially for the C1s peaks.

The same procedure was used to form a bR layer on the substrate for device fabrication, as described below in -2- below.

## ***2. Protein Junction fabrication***

300 nm of SiO<sub>x</sub>-on-Si wafer was cut into 1.5 × 1.5 cm<sup>2</sup> pieces, which were cleaned by ultra-sonication in acetone followed by isopropyl alcohol and water, for 10 min each. Cleaned SiO<sub>x</sub>/Si wafer pieces were used to make a pattern of 4 μm wide gold lines (3 nm Cr/50 nm Au) using standard photolithography microfabrication. The same conditions were used as detailed in section -1- to prepare a bR layer on the Au lines. After this step, 10 nm carbon was deposited using e-beam evaporation followed by 30 nm gold.

These junctions were used for I-V measurements with a two-probe configuration in a cryogenic probe station (LakeShore TTPX) at temperatures from 7-10K to 300K (using liquid He). In this probe station various temperature sensors are available to measure temperature, in the holder onto which the sample is placed, on the, probe and the probe arm. The lowest temperature of the sample (back of it) and the probe arm are found to be 10 K and 7 K, respectively. Thus, the lowest steady-state sample temperature (reached after equilibration, as for every temperature at which we measured) is given by its upper limit of 10K.

Impedance spectroscopy measurements were done at room temperature using an impedance analyzer (Zurich Instruments MFIA) in low vacuum ( $10^{-3}$  mbar);. The instrument was connected to the probe station in a two-probe configuration.

## Acknowledgements

We thank the nanofabrication unit at Chemical Reserch Support Department (WIS), specifically Messrs. Assaf Hazzan, Sharon Garusi and Leonid Tunik, for their valuable guidance and assistance with device fabrication. We thank Dr. Omer Yaffe for making impedance measurement facilities available to us. We are grateful to Drs. R. McCreery (U of Alberta) and J. A. Fereiro IISER TVM for useful discussions. SKS thanks the WIS Feinberg Graduate School for partial fellowship support. The work was supported by research grants from the Tom and Mary Beck Center for Advanced and Intelligent Materials, and from the Kimmelman Center for Biomolecular Structure and Assembly, all at the Weizmann Institute of Science, where MS holds the Katzir-Makineni Chair in Chemistry.

## References

- (1) Jiang, T.; Zeng, B.-F.; Zhang, B.; Tang, L. Single-Molecular Protein-Based Bioelectronics via Electronic Transport: Fundamentals, Devices and Applications. *Chem. Soc. Rev.* **2023**, *52* (17), 5968–6002.
- (2) Luo, L.; Choi, S. H.; Frisbie, C. D. Probing Hopping Conduction in Conjugated Molecular Wires Connected to Metal Electrodes. *Chem. Mater.* **2011**, *23* (3), 631–645.

- (3) Futera, Z.; Ide, I.; Kayser, B.; Garg, K.; Jiang, X.; van Wonderen, J. H.; Butt, J. N.; Ishii, H.; Pecht, I.; Sheves, M.; Cahen, D.; Blumberger, J. Coherent Electron Transport across a 3 Nm Bioelectronic Junction Made of Multi-Heme Proteins. *J. Phys. Chem. Lett.* **2020**, *11* (22), 9766–9774.
- (4) Fereiro, J. A.; Pecht, I.; Sheves, M.; Cahen, D. Inelastic Electron Tunneling Spectroscopic Analysis of Bias-Induced Structural Changes in a Solid-State Protein Junction. *Small* **2021**, *17* (19), 2008218.
- (5) Bostick, C. D.; Mukhopadhyay, S.; Pecht, I.; Sheves, M.; Cahen, D.; Lederman, D. Protein Bioelectronics: A Review of What We Do and Do Not Know. *Rep. Prog. Phys.* **2018**, *81* (2), 026601. <https://doi.org/10.1088/1361-6633/aa85f2>.
- (6) Slinker, J. D.; Muren, N. B.; Renfrew, S. E.; Barton, J. K. DNA Charge Transport over 34 Nm. *Nature Chemistry* **2011**, *3* (3), 228–233.
- (7) Gupta, N. K.; Karuppanan, S. K.; Pasula, R. R.; Vilan, A.; Martin, J.; Xu, W.; May, E. M.; Pike, A. R.; Astier, H. P. A. G.; Salim, T.; Lim, S.; Nijhuis, C. A. Temperature-Dependent Coherent Tunneling across Graphene–Ferritin Biomolecular Junctions. *ACS Appl. Mater. Interfaces* **2022**, *14* (39), 44665–44675.
- (8) Cahen, D.; Pecht, I.; Sheves, M. What Can We Learn from Protein-Based Electron Transport Junctions? *J. Phys. Chem. Lett.* **2021**, *12* (47), 11598–11603.
- (9) Chong, G. W.; Karbelkar, A. A.; El-Naggar, M. Y. Nature’s Conductors: What Can Microbial Multi-Heme Cytochromes Teach Us about Electron Transport and Biological Energy Conversion? *Current Opinion in Chemical Biology* **2018**, *47*, 7–17.
- (10) Bera, S.; Fereiro, J. A.; Saxena, S. K.; Chryssikos, D.; Majhi, K.; Bendikov, T.; Sepunaru, L.; Ehre, D.; Tornow, M.; Pecht, I.; Vilan, A.; Sheves, M.; Cahen, D. Near-Temperature-Independent Electron Transport Well beyond Expected Quantum Tunneling Range via Bacteriorhodopsin Multilayers. *J. Am. Chem. Soc.* **2023**, *145* (45), 24820–24835.
- (11) Morteza Najarian, A.; Bayat, A.; McCreery, R. L. Orbital Control of Photocurrents in Large Area All-Carbon Molecular Junctions. *J. Am. Chem. Soc.* **2018**, *140* (5), 1900–1909.
- (12) Morteza Najarian, A.; Szeto, B.; Tefashe, U. M.; McCreery, R. L. Robust All-Carbon Molecular Junctions on Flexible or Semi-Transparent Substrates Using “Process-Friendly” Fabrication. *ACS Nano* **2016**, *10* (9), 8918–8928.
- (13) He, T.; Friedman, N.; Cahen, D.; Sheves, M. Bacteriorhodopsin Monolayers for Optoelectronics: Orientation and Photoelectric Response on Solid Supports. *Advanced Materials* **2005**, *17* (8), 1023–1027.

- (14) Denkov, N. D.; Yoshimura, H.; Kouyama, T.; Walz, J.; Nagayama, K. Electron Cryomicroscopy of Bacteriorhodopsin Vesicles: Mechanism of Vesicle Formation. *Biophysical Journal* **1998**, *74* (3), 1409–1420.
- (15) Garg, K.; Raichlin, S.; Bendikov, T.; Pecht, I.; Sheves, M.; Cahen, D. Interface Electrostatics Dictates the Electron Transport via Bioelectronic Junctions. *ACS Appl. Mater. Interfaces* **2018**, *10* (48), 41599–41607.
- (16) Sepunaru, L.; Friedman, N.; Pecht, I.; Sheves, M.; Cahen, D. Temperature-Dependent Solid-State Electron Transport through Bacteriorhodopsin: Experimental Evidence for Multiple Transport Paths through Proteins. *J. Am. Chem. Soc.* **2012**, *134* (9), 4169–4176.
- (17) Bera, S.; Govinda, S.; Fereiro, J. A.; Pecht, I.; Sheves, M.; Cahen, D. Biotin Binding Hardly Affects Electron Transport Efficiency across Streptavidin Solid-State Junctions. *Langmuir* **2023**, *39* (4), 1394–1403.
- (18) Edman, K.; Nollert, P.; Royant, A.; Belrhali, H.; Pebay-Peyroula, E.; Hajdu, J.; Neutze, R.; Landau, E. M. High-Resolution X-Ray Structure of an Early Intermediate in the Bacteriorhodopsin Photocycle. *Nature* **1999**, *401* (6755), 822–826.
- (19) Yan, H.; Bergren, A. J.; McCreery, R. L. All-Carbon Molecular Tunnel Junctions. *J. Am. Chem. Soc.* **2011**, *133* (47), 19168–19177.
- (20) Bergren, A. J.; Zeer-Wanklyn, L.; Semple, M.; Pekas, N.; Szeto, B.; McCreery, R. L. Musical Molecules: The Molecular Junction as an Active Component in Audio Distortion Circuits. *J. Phys.: Condens. Matter* **2016**, *28* (9), 094011.
- (21) Saxena, S. K.; Tefashe, U. M.; McCreery, R. L. Photostimulated Near-Resonant Charge Transport over 60 Nm in Carbon-Based Molecular Junctions. *J. Am. Chem. Soc.* **2020**, *142* (36), 15420–15430.
- (22) Mukhopadhyay, S.; Karuppanan, S. K.; Guo, C.; Fereiro, J. A.; Bergren, A.; Mukundan, V.; Qiu, X.; Castañeda Ocampo, O. E.; Chen, X.; Chiechi, R. C.; McCreery, R.; Pecht, I.; Sheves, M.; Pasula, R. R.; Lim, S.; Nijhuis, C. A.; Vilan, A.; Cahen, D. Solid-State Protein Junctions: Cross-Laboratory Study Shows Preservation of Mechanism at Varying Electronic Coupling. *iScience* **2020**, *23* (5), 101099.
- (23) Das, S.; Citra Asmara, T.; Patra, A.; Song, Z.; Bista, S. S.; Somasundaran, P.; Rusydi, A.; Barbiellini, B.; Venkatesan, R. Optical Properties of Bacteriorhodopsin–Gold Bionano Interfaces. *J. Phys. Chem. C* **2019**, *123* (43), 26516–26521.

- (24) Seta, P.; Ormos, P.; D'Epenoux, B.; Gavach, C. Photocurrent Response of Bacteriorhodopsin Adsorbed on Bimolecular Lipid Membranes. *Biochimica et Biophysica Acta (BBA) - Bioenergetics* **1980**, *591* (1), 37–52.
- (25) Jin, Y.; Friedman, N.; Sheves, M.; He, T.; Cahen, D. Bacteriorhodopsin (bR) as an Electronic Conduction Medium: Current Transport through bR-Containing Monolayers. *Proceedings of the National Academy of Sciences* **2006**, *103* (23), 8601–8606.
- (26) Jin, Y. D.; Friedman, N.; Sheves, M.; Cahen, D. Bacteriorhodopsin-Monolayer-Based Planar Metal–Insulator–Metal Junctions via Biomimetic Vesicle Fusion: Preparation, Characterization, and Bio-Optoelectronic Characteristics. *Advanced Functional Materials* **2007**, *17* (8), 1417–1428.
- (27) Mukhopadhyay, S.; Cohen, S. R.; Marchak, D.; Friedman, N.; Pecht, I.; Sheves, M.; Cahen, D. Nanoscale Electron Transport and Photodynamics Enhancement in Lipid-Depleted Bacteriorhodopsin Monomers. *ACS Nano* **2014**, *8* (8), 7714–7722.
- (28) Mukhopadhyay, S.; Dutta, S.; Pecht, I.; Sheves, M.; Cahen, D. Conjugated Co-factor Enables Efficient Temperature-Independent Electronic Transport Across ~6 Nm Long Halorhodopsin. *J. Am. Chem. Soc.* **2015**, *137* (35), 11226–11229.
- (29) Chen, X.; Nijhuis, C. A. The Unusual Dielectric Response of Large Area Molecular Tunnel Junctions Probed with Impedance Spectroscopy. *Advanced Electronic Materials* **2022**, *8* (2), 2100495.